

THE INFLUENCE OF ISOTHERMAL AGEING AND SUBSEQUENT HYDROGEN CHARGING AT ROOM TEMPERATURE ON LOCAL MECHANICAL PROPERTIES AND FRACTURE CHARACTERISTICS OF MARTENSITIC-BAINITIC WELDMENTS FOR POWER ENGINEERING

L. Falat^a, L. Čiripová^a, V. Homolová^{a,*}, A. Kroupa^b

^aInstitute of Materials Research, Slovak Academy of Sciences, Košice, Slovak Republic

^bInstitute of Physics of Materials, Academy of Sciences of the Czech Republic, Brno, Czech Republic

(Received 15 May 2017; accepted 22 September 2017)

Abstract

The present study deals with the effects of high temperature expositions and subsequent cathodic hydrogen charging of dissimilar martensitic/bainitic weldment on its local mechanical properties and fracture behaviour at room temperature. Circumferential welded joint under investigation was produced by tungsten inert gas welding of X10CrWMoVNb9-2 martensitic and 7CrMoVTiB10-10 bainitic steels tubes with Ni-based filler metal and the application of subcritical post-weld heat treatment. Hardness profile measurements revealed pronounced hardness peaks in over-heated regions of the individual steels heat-affected zones which remained preserved also during subsequent expositions at 600°C for up to 5000 hours. Gradual microstructural degradation of these regions included precipitate coarsening and the formation of new secondary phases during thermal exposure. The combined effects of thermal and hydrogen embrittlement of the studied weldment resulted in deleterious effects on its tensile and fracture behaviour.

Key words: Power-plant steels; Dissimilar weld; Thermal exposure; Hydrogen charging; Mechanical properties; Fracture mechanism

1. Introduction

Sustainable socio-economic development requires continuous increase in electric power production as well as protection of global environment. Besides alternative energy sources, a possible way allowing gradual increase in energy production with simultaneous decrease of CO₂ emissions is based on the increasing of steam-cycle thermal efficiency of modern power generating plants. This issue represents the main driving force for new material developments aiming for obtaining higher operating conditions in so-called “ultra supercritical” boilers [1-3]. Since the power plant boilers consist of several steam circuits heated up to different service temperatures, a wide range of creep-resistant steels is used for their construction. The Fe-Cr-Mo-V-W-based ferritic/martensitic steels and their welds are frequently used in both coal-fired and nuclear plants for construction of various parts of power generation equipment [1,4]. In view of mechanical and thermal loading and risk of potential failure, the welded joints

unavoidable in construction of boiler equipment, belong to its most critical parts [5,6]. Furthermore, distinct zones of the weldments such as base material (BM), weld metal (WM) and heat-affected zone (HAZ) undergo their own specific degradation in service or laboratory test conditions [6,7]. In the case of transition weldments between different steel grades, the situation is even more complicated due to redistribution effects of alloying elements and grain size characteristics along the weld metal/base metal interfaces [8-11]. Typical examples represent dissimilar welded joints between 9Cr martensitic and 2.25Cr bainitic steels interconnecting superheater circuit with steam evaporator i.e. membrane water walls system. Some studies e.g. [8,11] focused on high temperature performance of dissimilar welds between the higher and lower chromium steels indicated a formation of carbon-depleted zones (“white bands”) at the lower alloyed weld side, resulting in their mechanical properties deterioration. Apart from long-term thermal degradation of boiler steels welded joints, the hydrogen-induced cold

Dedicated to the memory of Professor Dragana Živković

* Corresponding author: vhomolova@saske.sk



cracking phenomena may be of another concern in power plants during their regular or accidental shut-downs. It is well-known that in tensile stress conditions, the hydrogen dissolved in high-strength steels may lead to hydrogen-assisted cracking [12-14]. The interpretation of various manifestations of hydrogen embrittlement has been described e.g. in [15] by several hydrogen acting mechanisms, such as hydrogen enhanced decohesion (HEDE), hydrogen enhanced localized plasticity (HELP), adsorption induced dislocation emission (AIDE) and hydrogen enhanced strain induced vacancy formation (HESIV). Nevertheless, because of considerable complexity of individual materials, environmental and loading conditions, it is important to study each case of hydrogen-assisted failure separately.

Our previous works [16,17] were dealing with the effects of cathodic hydrogen charging on local mechanical properties and fracture characteristics of transition welded joints between several ferritic and austenitic creep-resistant steels. The present study is focused on the effects of long-term isothermal ageing and subsequent hydrogen charging on local mechanical properties and fracture performance of Ni-based transition weldment between X10CrWMoVNb9-2 martensitic and 7CrMoVTiB10-10 bainitic power plant steels.

2. Experimental procedure

The tubes of X10CrWMoVNb9-2 (T92 Grade) martensitic and 7CrMoVTiB10-10 (T24 Grade) bainitic steels with their outer diameter of 38 mm and wall thickness of 5.6 mm were welded using tungsten inert gas method and Ni-based filler metal Nirod 600. This innovative approach was used in order to suppress diffusion of interstitial elements between the welded dissimilar materials. Table 1 shows chemical composition of individual materials used for fabrication of studied experimental welded joints.

After the manufacture, the weldments were processed by subcritical post-weld heat treatment (PWHT) regime at 720°C for 2 hours with subsequent cooling within laboratory resistance furnace. The initial PWHT state represented the reference material state. Afterwards, two separate series of the weldments were isothermally aged at 600°C for 1000 hours and 5000 hours, respectively. A variation of local mechanical properties across the weldments in

all heat-treated states (i.e. PWHT, 600°C/1000 h, and 600°C/5000 h) was determined by HV10 hardness profile measurements at ambient temperature. Microstructural and local mechanical characteristics of individual over-heated regions of the both steels heat-affected zones (HAZ) were studied in dependence of ageing time by means of conventional metallography (i.e. light-optical microscopy and scanning electron microscopy) and notch tensile tests. In order to predict equilibrium phases in thermally aged welds, thermodynamic calculations were employed using the program Thermo-Calc [18]. The TCFE6, STEEL16 and TCNI8 thermodynamic databases were used in equilibrium phase calculations for T92, T24 and Nirod 600 materials, respectively. For conducting of the tensile tests on TIRATEST 300 universal testing machine, the M6 round tensile test samples with 4 mm in body diameter and 40 mm of gauge length were used. The samples were alternatively “V”-notched in individual over-heated HAZ regions, i.e. either in T92 martensitic or T24 bainitic steel part (see Fig. 1).

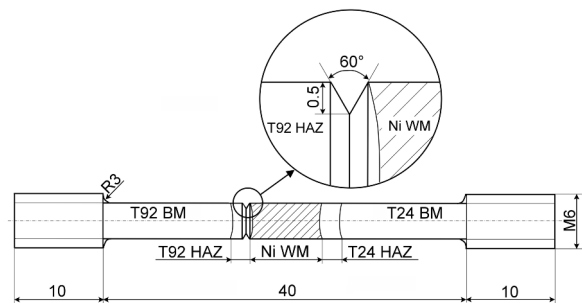


Figure 1. Non-standard tensile sample with circumferential V-notch in over-heated HAZ. (Notch root radius was 0.2 mm. For the local mechanical properties estimation, either T92 HAZ or T24 HAZ was V-notched).

One half of all prepared tensile samples was tensile tested without hydrogen charging. The second half of the samples was cathodically hydrogen charged at room temperature just before conducting the tensile tests. The hydrogen charging was carried out for 24 hours in a solution of 1M HCl with 0.1N $N_2H_6SO_4$ at a current density of 200 A.m⁻². The experimental procedure was optimized in our previous works [16,17] which estimated full hydrogen saturation of tensile specimens after 24 hours of

Table 1. Chemical composition in mass % of individual materials used for preparation of dissimilar martensitic/bainitic welded joints with Ni-based weld metal (Ni WM)

	C	N	Si	Mn	Cr	Mo	W	B	Ni	Al	V	Nb	Ti	Fe
X10CrWMoVNb9-2 (T92)	0.11	0.056	0.38	0.49	9.08	0.31	1.57	0.0023	0.33	0.014	0.2	0.069	-	Balance
7CrMoVTiB10-10 (T24)	0.08	0.007	0.21	0.53	2.44	0.95	-	0.0042	0.18	-	0.36	0.002	0.053	Balance
Ni WM (Nirod 600)	0.05	-	0.3	3	20	-	-	-	Balance	-	-	2	-	2



cathodic charging. Subsequently, the hydrogen charged specimens were tensile tested at ambient temperature at a strain rate of $2.1 \times 10^{-4} \text{ s}^{-1}$ enabling the study of hydrogen effect in accelerated tensile loading conditions. From three individual tensile tests for each material state, the average values of notch tensile strength (R_{m_v}) and reduction of area under the notch (RA_v) were obtained. Microstructural analyses and fractography of tensile tested specimens were performed by light optical microscopy (Olympus GX 71) and scanning electron microscopy (SEM - JEOL JSM - 7000F) equipped with energy dispersive X-ray (EDX - INCA X-sight model 7557) spectrometer.

3. Results and discussion

3.1 Microstructures and hardness measurements

Fig. 2 shows light-optical microstructures of T92 HAZ tempered martensitic regions of the studied weldment in its initial PWHT state (Fig. 2a) and after its longest thermal exposure at 600°C for 5000 h (Fig. 2b). On the other hand, Fig. 3 shows light-optical microstructures of T24 HAZ tempered bainitic regions of the studied weldment in its initial PWHT state (Fig. 3a) and after its longest thermal exposure at 600°C for 5000 h (Fig. 3b).

It can be clearly seen, that there are significant differences between the martensitic and bainitic HAZ microstructures in both the depicted material states. These differences are noticeable for prior austenitic grain size and the density of secondary phase precipitates. Obviously, the higher precipitate density in martensitic T92 steel HAZ regions (Fig. 2) resulted in lower grain size, compared to the bainitic T24 steel HAZs (Fig. 3). This observation can be directly related to the intergranular precipitates pinning effects resulting in hindering the mobility of grain boundaries during the weld preparation, its PWHT processing and subsequent thermal exposure. Microstructural changes which occur in both the HAZ regions during isothermal expositions are generally related to additional precipitation and coarsening of secondary phase particles. Thermodynamic calculations were performed in order to predict equilibrium phases in thermally aged weldments (see Fig. 4).

In accordance with Table 1, the positions of T92 and T24 steels phase compositions within the whole temperature range of the calculated phase diagrams correspond to their individual isoplethal sections at 0.11 and 0.08 mass % C, respectively. The calculated temperature intervals of thermodynamic stability of individual phases for T92 and T24 steels are shown in Table 2 and Table 3, respectively.

According to the performed thermodynamic calculations, the following secondary precipitate phases in T92 material are to be expected at 600°C in equilibrium: MX (M = V, Nb; X = C, N), Cr-rich

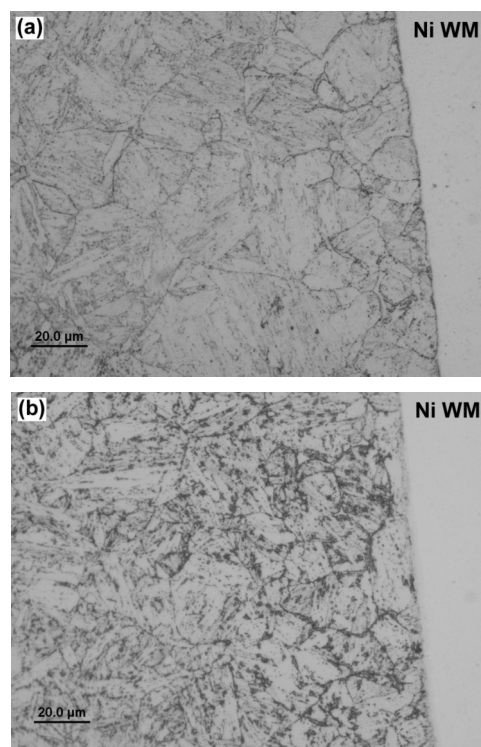


Figure 2. Light-optical micrographs of T92 HAZ of investigated welded joint in: (a) PWHT state and (b) isothermally aged state at 600°C for 5000 h.

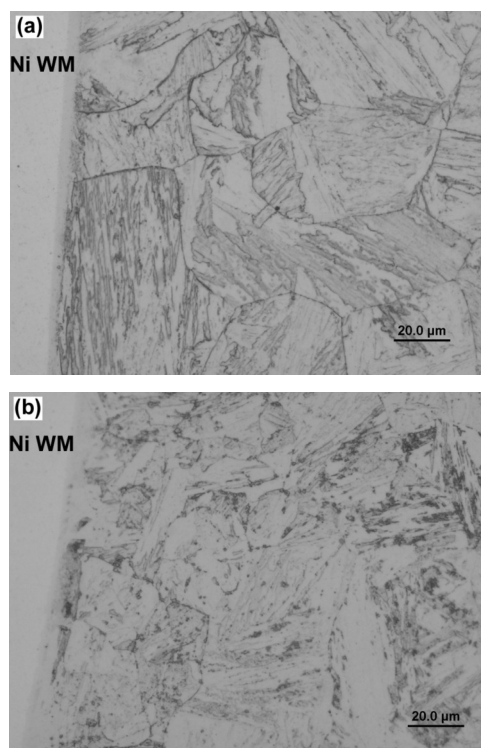


Figure 3. Light-optical micrographs of T24 HAZ of investigated welded joint in: (a) PWHT state and (b) isothermally aged state at 600°C for 5000 h.

$M_{23}C_6$ and $Fe_2(W,Mo)$ based Laves phase (Fig. 4a). On the other hand, the expected secondary phases in T24 material at 600°C are the following: MX (M = V, Nb; X = C, N), Cr-rich M_7C_3 and Mo-rich M_6C (Fig. 4b). Characterization of microstructures and mechanical properties of advanced martensitic and bainitic creep-resistant steels and their welds in PWHT state and after long thermal exposures has been extensively reported in literature, e.g. [19-24]. In the present study, microstructural analyses and secondary precipitates differentiation were conducted by means of SEM observations using both secondary electrons and back-scattered electrons visualization (Fig. 5 and Fig. 6). The SEM micrographs in Fig. 5 and Fig. 6 show microstructural changes after the long-term ageing at 600°C for 5000 h. In agreement with former studies [19, 23] and performed

calculations (Fig. 4), these changes involve coarsening of original Cr-rich carbides ($M_{23}C_6$ and M_7C_3) as well as the additional formation and coarsening of $Fe_2(W,Mo)$ based Laves phase and Mo-rich M_6C carbides in T92 and T24 HAZs, respectively.

The phases rich in W and/or with Mo possess high average atomic numbers and thus brighter phase contrast on the SEM images visualized by back-scattered electrons (BSE) contrast (Fig. 5b and Fig. 6b). On the contrary, the carbide and/or carbo-nitride phases with lower average atomic numbers exhibit less-pronounced greyish BSE contrast. The BSE-contrast between the „greyish“ Cr-rich carbides and similarly „greyish“ matrix was rather insignificant due to their quite similar average atomic numbers.

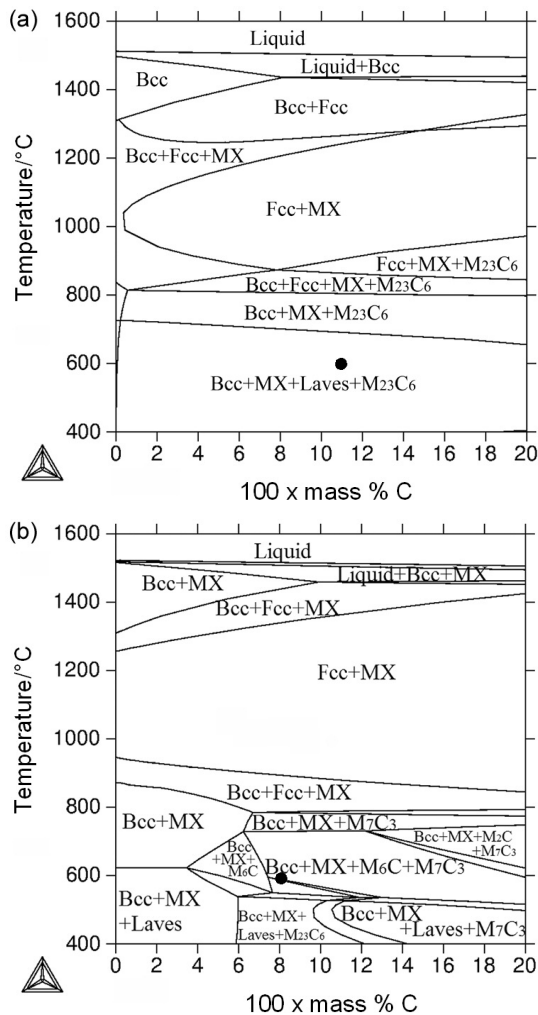


Figure 4. Equilibrium phase diagrams showing the occurrence of stable phases in: (a) T92 steel and (b) T24 steel. (Full circles in the diagrams depict the positions corresponding to stable phase compositions of individual steels at 600°C.)

Table 2. Calculated temperature ranges for equilibrium phases in T92 material

Temperature range/°C	Thermodynamically stable phases
400-693	BCC, MX, Laves, $M_{23}C_6$
693-803	BCC, MX, $M_{23}C_6$
803-862	BCC, MX, FCC, $M_{23}C_6$
862-906	FCC, MX, $M_{23}C_6$
906-1240	FCC, MX
1240-1265	BCC, FCC, MX
1265-1430	BCC, FCC
1430-1436	L, BCC, FCC
1436-1501	L, BCC
above 1501	L

Table 3. Calculated temperature ranges for equilibrium phases in T24 material

Temperature range/°C	Thermodynamically stable phases
400-532	BCC, MX, Laves, $M_{23}C_6$
532-547	BCC, MX, Laves, $M_{23}C_6$, M_6C
547-586	BCC, MX, $M_{23}C_6$, M_6C
586-588	BCC, MX, $M_{23}C_6$, M_6C , M_7C_3
588-728	BCC, MX, M_6C , M_7C_3
728-782	BCC, MX, M_7C_3
782-785	BCC, MX, M_7C_3 , FCC
785-892	BCC, MX, FCC
892-1338	MX, FCC
1338-1439	BCC, MX, FCC
1439-1470	BCC, MX
1470-1507	L, BCC, MX
1507-1515	L, BCC
above 1515	L

The dark areas in Fig. 6 represent the holes originated from local over-etching.

Phase analysis of the Nirod 600 alloy was carried out in our former study focused on Ni-based transition weldment between T92 and TP316H creep-resistant steels [25] and only NbC type intragranular and intergranular carbides were indicated in the used Ni-based weld metal. In the study focused on dissimilar T91/TP316H welds characterisation, Blach et al. [17] indicated for Thermit Nicro 82 weld metal (chemically similar to Nirod 600) the occurrence of (Nb,Ti)C and Cr₂₃C₆ carbides in grain interiors and grain boundaries, respectively. The estimation of local mechanical properties variation across the studied T92/T24 welded joint in individual material states was performed by HV10 hardness measurements (Fig. 7).

The hardness profiles in Fig. 7 clearly show that the over-heated T92 and T24 HAZs regions represent always the most critical parts of studied welded joints because of their significant hardness peaks related to the locally highest transformation (martensitic) hardening. This enhanced local strengthening occurs due to the highest peak temperatures reached during the welding, resulting in maximum alloying effects before subsequent matrix martensitic transformation [26]. This observation agrees well with the results of

similar studies focused on characterization of mechanical properties of welded joints prepared by fusion welding techniques e.g. [27]. The Ni WM (Nirod 600) with its fully recrystallized Ni-based austenitic microstructure exhibited the lowest hardness values in PWHT state. Its gradual hardness increase with increasing ageing duration can likely be related to additional precipitation of thermally stable secondary phases. Apart from aforementioned carbides [25], the observed strengthening of Ni WM

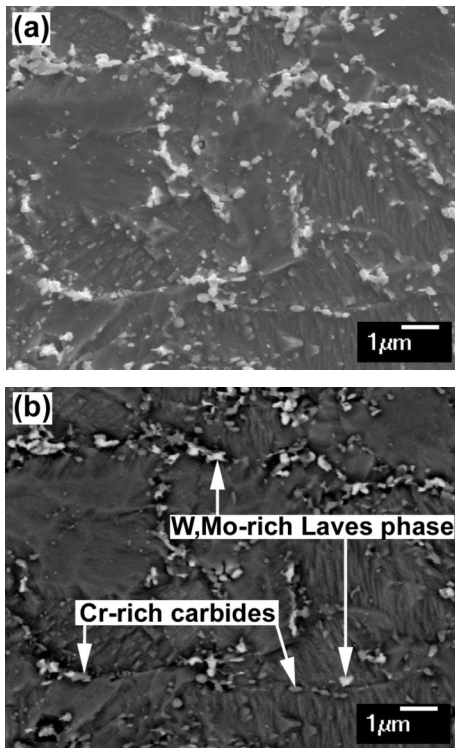


Figure 5. SEM-micrographs of isothermally aged T92 HAZ at 600°C for 5000 h, visualized in the mode of: (a) secondary electrons and (b) back-scattered electrons.

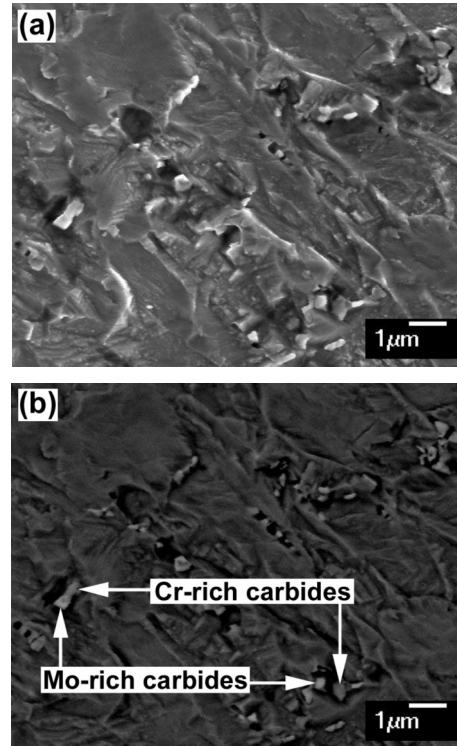


Figure 6. SEM-micrographs of isothermally aged T24 HAZ at 600°C for 5000 h, visualized in the mode of: (a) secondary electrons and (b) back-scattered electrons.

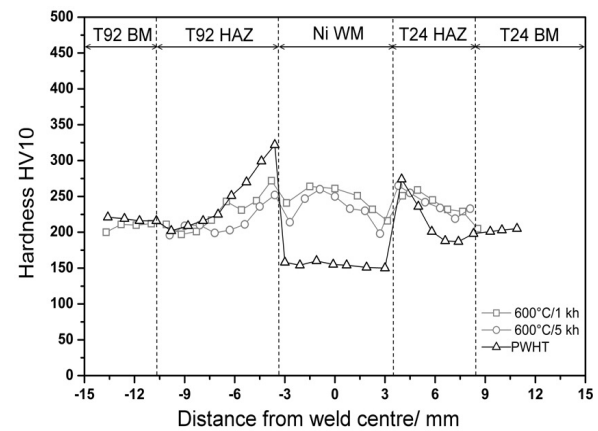


Figure 7. Cross-weld hardness profiles of T92/T24 welded joints in their individual material states.

during thermal exposure (Fig. 7) might also be caused by additional intermetallic phase formation. Since the hardness is much lower at fusion boundaries (Fig. 7), it can be assumed that the central part of Ni WM contains much more niobium than carbon and the niobium and nickel form together intermetallic phase. Indeed, thermodynamic calculation of temperature dependence of stable phases in Nirod 600 weld metal (Fig. 8) predicted the existence of intermetallic Ni_3Nb precipitates at 600°C . Their experimental determination including detailed characterization of their homogeneity range and ageing performance will be the subject of our subsequent studies.

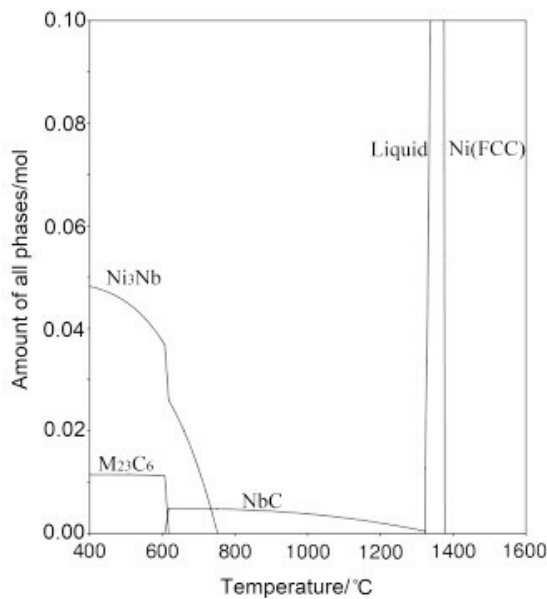


Figure 8. Equilibrium phase diagram showing the amount of stable phases in Nirod 600 weld metal depending on temperature.

3.2 Tensile properties and fractographic observations

The characterization of notch tensile properties of distinct HAZ regions of investigated martensitic/bainitic weldments in their individual material states is shown in Figs. 9 and 10. Fig. 9a shows the values of notch tensile strength (R_{mV}) for T92 HAZ region in all heat treated material states (PWHT, $600^\circ\text{C}/1000\text{ h}$, $600^\circ\text{C}/5000\text{ h}$) tested in conditions either without or with application of hydrogen charging. Similarly, Fig. 9b depicts R_{mV} values of T24 HAZ in its individual heat treated states (PWHT, $600^\circ\text{C}/1000\text{ h}$, $600^\circ\text{C}/5000\text{ h}$) in conditions without as well as with hydrogen charging.

From Fig. 9 it is obvious that the effect of thermal exposure at 600°C on R_{mV} values of both T24 and T92 HAZs is characterized by their slight initial

increase after 1000 h of ageing at 600°C . However, further ageing up to 5000 h resulted in gradual decrease of R_{mV} values of both T24 and T92 HAZs. The observed behaviour can be explained in terms of secondary hardening related to the additional fine precipitation of MX and Laves phase in T92 HAZ and MX and Mo_2C in T24 HAZ [19, 23]. Subsequent decrease of strength can be ascribed to further coarsening of intergranular Cr-rich carbides (M_7C_3 and $M_{23}C_6$), additional precipitation and coarsening of $Fe_2(W,Mo)$ based Laves phase in T92 HAZ and Mo-rich M_6C carbides in T24 HAZ, besides on-going recovery processes of their individual tempered microstructures (Fig. 5 and Fig. 6). Regarding the effect of hydrogen charging it can be stated that it resulted in visible hardening in both T92 and T24 HAZs. The observed hardening can be related to pinning effects between hydrogen and free dislocations and/or precipitate/matrix interfaces in tempered martensitic T92 HAZ and tempered bainitic T24 HAZ microstructures.

It seems that the hardening of T92 HAZ by hydrogen is more significant than in the case of hydrogen charged T24 HAZ (Fig. 9) which may be presumably related to higher initial dislocation density and significantly higher precipitation density of T92 HAZ compared to T24 HAZ (Fig. 5 and Fig. 6).

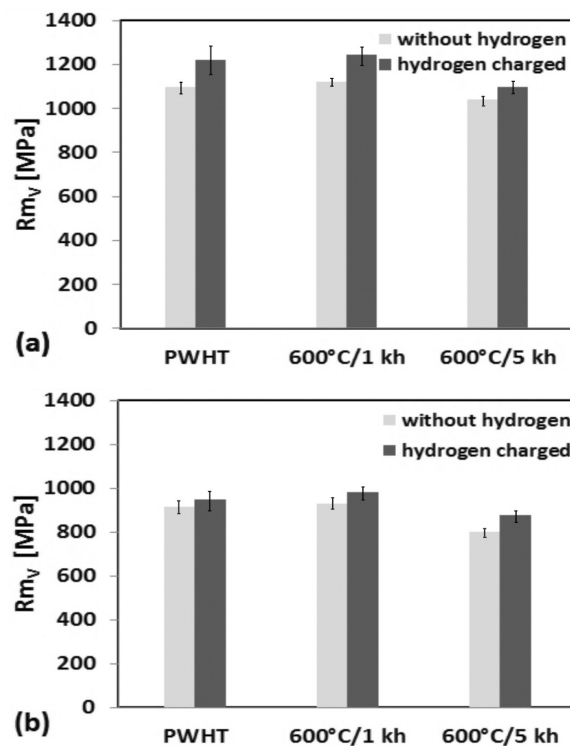


Figure 9. Notch tensile strength of individual HAZ regions of T92/T24 welded joints in their individual material states: (a) T92 HAZ and (b) T24 HAZ (R_{mV} values according to [28]).

Fig. 10 shows the values of reduction of area under the notch (RA_V) for both T92 and T24 HAZs in all heat treated material states (PWHT, 600°C/1000 h, 600°C/5000 h), tested in conditions either without or with application of hydrogen charging.

Regardless of hydrogen charging application, the dependencies of RA_V values on ageing time always show simple monotonous decreasing which can be generally related to the coarsening of secondary phase precipitates during long-term ageing [29]. Additional detrimental effects of hydrogen charging on the resulting RA_V values of both the HAZ regions are more complex than in the case of thermal degradation of individual HAZs microstructures. There are several different microstructural objects in steels such as free dislocations, grain/subgrain boundaries, precipitates and inclusions which may act like either reversible or irreversible hydrogen traps [14]. Such hydrogen trapping may have crucial effects on the resulting mechanical properties and fracture behaviour [30-33]. From Fig. 10 it can be concluded that additional hydrogen charging of thermally aged weldments resulted in further decrease of RA_V values of both their HAZ regions.

Fracture surfaces of broken tensile specimens after the notch tensile tests of the investigated welded joints in respective material states regarding the heat treatment and hydrogen charging application are

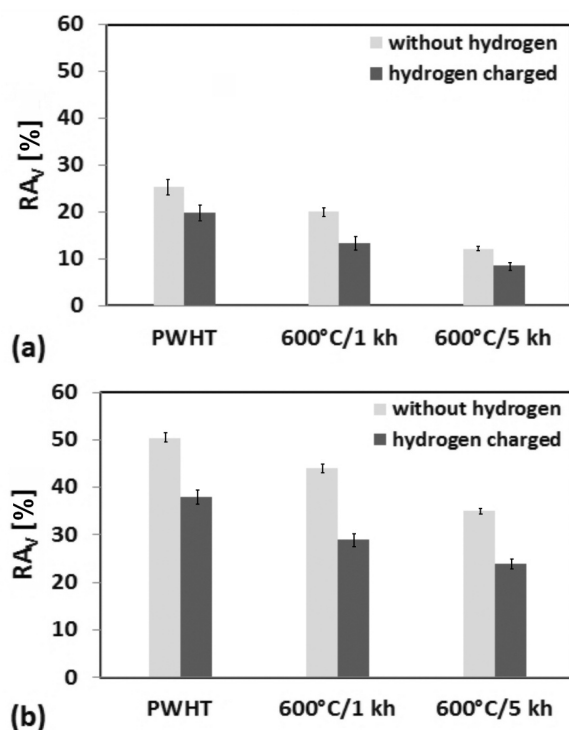


Figure 10. Reduction of area under the notch of individual HAZ regions of T92/T24 welded joints in their individual material states: (a) T92 HAZ and (b) T24 HAZ (RA_V values according to [28]).

shown in Figs. 11-13. Fig. 11 shows SEM-fractographs of T92 and T24 HAZs in their original PWHT condition, i.e. without the application of hydrogen charging.

Both the fractures are characterized by clearly visible ductile dimple areas, however, the T92 HAZ (Fig. 11a) exhibits also some small fraction of transgranular quasi-cleavage locations. On the other hand, the fracture surface of T24 HAZ (Fig. 11b) exhibits besides the dimples a significant portion of large cavities that indicate weld imperfections.

Fig. 12a indicates that after the long-term ageing at 600°C for 5000 hours, the fracture characteristics of T92 HAZ changed from the original ductile dimple fracture in PWHT state (Fig. 11a) to the mixed fracture of transgranular quasi-cleavage and certain fraction of intergranular decohesion. The occurrence of intergranular fracture areas on long-term isothermally aged T92 HAZ can be directly related to intensive precipitation and coarsening of both $M_{23}C_6$ carbides and $Fe_2(W, Mo)$ Laves phase on grain and subgrain boundaries (Fig. 5). On the other hand, the same conditions of thermal exposure (600°C/5000 h) of T24 HAZ resulted in fracture characteristics consisting of ductile dimples and some signs of quasi-cleavage fracture areas originating on large secondary phase precipitates and/or inclusions (Fig. 12b). The

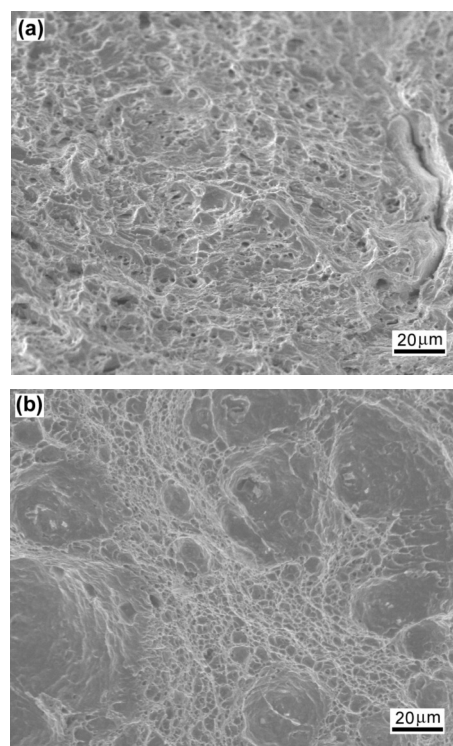


Figure 11. Fracture surface morphology of distinct HAZ regions of T92/T24 welded joint in its PWHT state after the tensile test at ambient temperature without hydrogen charging: (a) T92 HAZ and T24 HAZ (b).

fractographs in Fig. 12 indicate the possible mechanisms responsible for the plasticity degradation to be decohesion at precipitate/matrix interfaces and/or cracking of coarse secondary particles during straining.

The combined effects of thermal and hydrogen embrittlement of T92 and T24 HAZs of the studied weldment are visualized in Fig. 13. The both depicted fracture surfaces show typical signs of hydrogen embrittlement related to specific transgranular cleavage characteristics with typical “crows-feet” marks and “fish-eyes” on the fracture surfaces of T92 and T24 HAZs, respectively.

The observed fracture features of individual HAZs correlate with their corresponding microstructures (Figs. 5, 6) and mechanical properties (Figs. 9, 10). It should be noted that microstructural evolution due to isothermal ageing may result in increasing amount of irreversible hydrogen traps (newly formed fine particle/matrix interfaces) and decreasing amount of reversible hydrogen traps (mainly free dislocations). However, the role of secondary phase precipitates may be twofold. The fine precipitates act like hydrogen embrittlement suppressors. On the other hand, it has been reported [33,34] that significant coarsening of secondary phase precipitates may lead to enhanced level of local hydrogen concentration

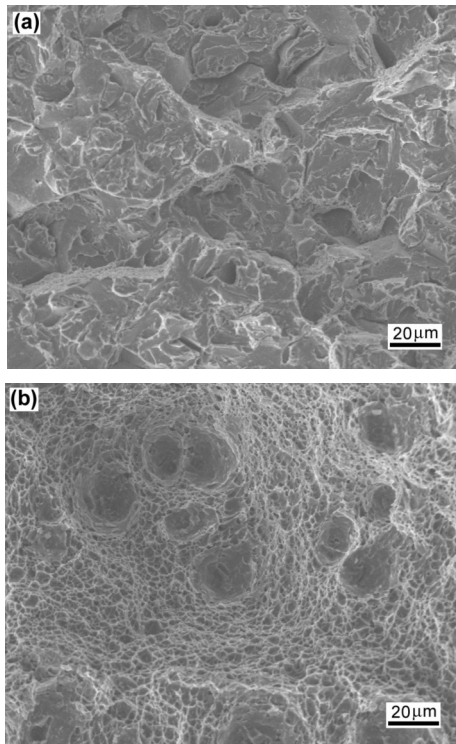


Figure 12. Fracture surface morphology of distinct HAZ regions after the room-temperature tensile test of isothermally aged T92/T24 welded joint at 600°C for 5000 h without hydrogen charging: (a) T92 HAZ and T24 HAZ (b).

exceeding its critical value for the crack propagation. For instance, Fig. 14 shows the effects of coarse precipitates acting like crack nucleation sites for hydrogen-assisted cracking in individual hydrogen-charged and tensile-strained HAZ regions.

With regard to the obtained results of tensile tests (Figs. 9, 10) and fractographic observations (Figs. 11-14) it can be concluded that both the T92 and T24 HAZs exhibited notable signs of hydrogen embrittlement in experimental conditions applied in the current study. For detailed characterisation of reversible and irreversible hydrogen trapping, thermal desorption analyses (TDA) are planned in our future investigations.

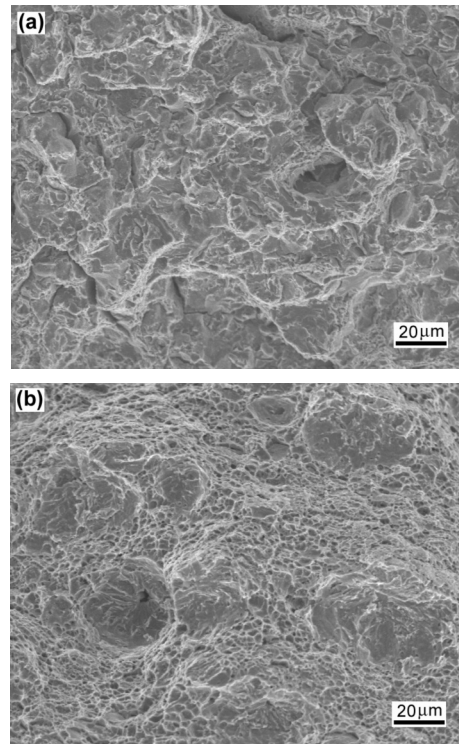


Figure 13. Fracture surface morphology of distinct HAZ regions after the room-temperature tensile test of isothermally aged T92/T24 welded joint at 600°C for 5000 h with hydrogen charging: (a) T92 HAZ and T24 HAZ (b).

4. Summary and conclusions

Dissimilar T92/T24 martensitic/bainitic weldments were investigated in terms of their HAZs microstructures and mechanical properties evolution during long-term ageing. Notch tensile tests of all heat-treated material states were conducted for both hydrogen-free and hydrogen-charged specimens. From the obtained results, following conclusions could be drawn:

Cross-weld hardness measurements of

investigated welded joints revealed sharp hardness gradients in both T92 and T24 HAZs that remained preserved during long-term ageing at 600°C up to 5000 h. The hardness peaks in over-heated regions are related to the locally highest transformation hardening effects thanks to maximum alloying (matrix supersaturation) at the highest peak temperatures reached during the welding, followed by subsequent transformation.

In agreement with performed thermodynamic calculations, the applied ageing effects on individual microstructures of studied martensitic/bainitic weldment resulted in gradual coarsening of Cr-rich ($M_{23}C_6$ and M_7C_3) carbides accompanied by additional precipitation of $Fe_2(W,Mo)$ Laves phase and M_6C carbides in T92 and T24 HAZs, respectively.

Ageing effects without hydrogen charging on local tensile properties of both the HAZs regions of studied T92/T24 weldment were manifested by clear initial increase of their Rm_V values after 1000 h of thermal exposure at 600°C. The increase of ageing time up to 5000 h resulted in notable decrease of Rm_V values due to secondary precipitates coarsening.

The plasticity of both the HAZs regions, represented by their RA_V values, exhibited only decreasing tendency with increasing time of thermal expositions. This behaviour can be likely ascribed to the effects of thermal degradation of individual HAZs microstructures related

mainly to precipitate coarsening. The possible mechanisms of plasticity deterioration were indicated on fracture surfaces to be decohesion at precipitate/matrix interfaces and/or cracking of coarse secondary particles during straining.

In comparison to the weldments without hydrogen charging, the hydrogen charged ones exhibited somewhat higher Rm_V values and clearly lower RA_V values for both the T92 and T24 HAZs in all their heat treated material states.

The differences between hydrogen-free and hydrogen-charged RA_V values were always higher for T24 HAZ that indicated its higher hydrogen embrittlement susceptibility compared to T92 HAZ. The observed behaviour is likely related to the lower precipitate density in T24 HAZ and thus lower amount of irreversible hydrogen traps compared to more hydrogen resistant T92 HAZ.

Fractographic observations revealed ductile dimple fracture features for both hydrogen-free, tensile tested T92 and T24 HAZs. In addition, T24 HAZ exhibited large cavities besides the dimples. Subsequent ageing at 600°C resulted in specific fractographic changes of T92 HAZ resulted in a mixture of transgranular quasi-cleavage and some intergranular decohesion. In contrast, T24 HAZ fracture preserved some ductile dimple features besides newly formed quasi-cleavage fracture areas.

Combined effects of isothermal pre-ageing and subsequent hydrogen charging resulted in specific transgranular quasi-cleavage fracture features of tensile tested T92/T24 welded joints, showing hydrogen embrittlement related “crows-feet” and “fish-eyes” patterns on T92 and T24 HAZs fracture surfaces, respectively. The observed fractographic manifestations of individual HAZ regions correspond well with their local microstructures and mechanical properties.

Acknowledgements

Financial support of present work by Slovak Scientific Grant Agency (VEGA) under the Grants Nos. 2/0151/16 and 2/0153/15 is gratefully acknowledged.

References

- [1] M. Igarashi, in Creep-resistant steels (F. Abe, T.-U. Kern, R. Viswanathan), Woodhead Publishing Ltd, Cambridge, 2008, p.539-572.
- [2] P. Bekeč, L. Parilák, P. Beraxa, M. Mojžiš, L. Domovcová, M. Fujda, Mater. Sci. Forum, 891 (2017) 167-170.
- [3] A. Fedoriková, T. Kvačkaj, R. Kočiško, R. Bidulský, P. Petroušek, J. Bidulská, L. Domovcová, Acta Metall. Slovaca, 22 (2) (2016) 102-110.
- [4] A. Udovsky, O. Fabrichnaya, J. Min. Metall. Sect. B-Metall., 52 (2) B (2016) 185-188.

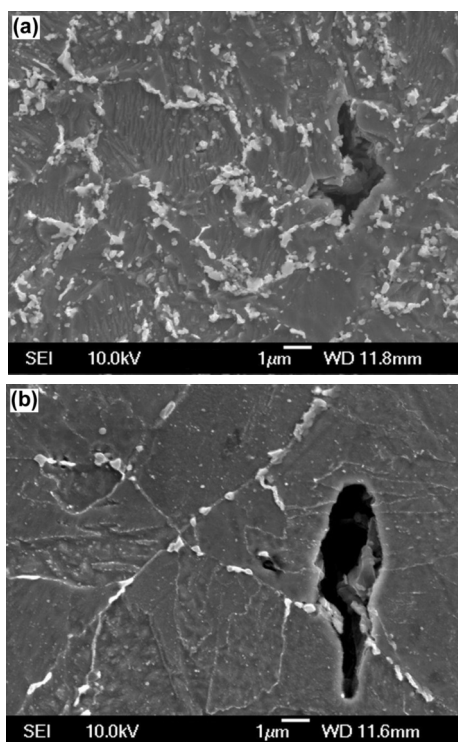


Figure 14. The occurrence of cracks in hydrogen charged and tensile tested HAZ microstructures of thermally aged T92/T24 weldment: T92 HAZ (a) and T24 HAZ (b).



- [5] V. Sklenička, K. Kuchařová, M. Svobodová, M. Kvapilová, P. Král, L. Horváth, *Mater. Character.*, 119 (2016) 1-12.
- [6] M. Sroka, A. Zieliński, M. Dziuba-Kaluza, M. Kremzer, M. Macek, A. Jasiński, *Metals*, 7 (3) (2017) Article number 82.
- [7] A. Janča, J. Siegl, P. Haušild, *J. Nucl. Mater.*, 481 (2016) 201-213.
- [8] L. Střílková, J. Holešinský, A. Maslova, Z. Kuboň, V. Vodárek, *Mater. Sci. Forum*, 782 (2014) 319-324.
- [9] L. Falat, V. Homolová, L. Čiripová, P. Ševc, M. Svoboda, *Adv. Mater. Sci. Eng.*, 2017 (Article ID 6824385) (2017) 14 pages.
- [10] E. Ranjbarnodeh, S. Serajzadeh, A.H. Kokabi, A. Fischer, *J. Min. Metall. Sect. B-Metall.* 51 (1) B (2015) 61-66.
- [11] Q. Wu, F. Lu, H. Cui, X. Liu, P. Wang, Y. Gao, *Mater. Lett.* 141 (2015) 242-244.
- [12] C. Pandey, N. Saini, M.M. Mahapatra, P. Kumar, *Int. J. Hydrogen Energy*, 41 (39) (2016) 17695-17712.
- [13] M. Rhode, J. Steger, E. Steppan, T. Kannengiesser, *Weld World*, 60 (4) (2016) 623-638.
- [14] G. Rosenberg, I. Sinaiova, *Mater. Sci. Eng. A*, 682A (2017) 410-422.
- [15] Q. Liu, A. Atrens, *Corros. Rev.*, 31 (3-6) (2013) 85-103.
- [16] J. Blach, L. Falat, *High Temp. Mater. Proc.*, 33 (4) (2014) 329-337.
- [17] J. Blach, L. Falat, P. Ševc, *Eng. Fail. Anal.*, 18 (1) (2011) 485-491.
- [18] www.thermocalc.se
- [19] A. Zielinski, G. Golanski, M. Sroka, *Kovove Mater.*, 54 (1) (2016) 61-70.
- [20] P. Mohyla, Z. Kubon, R. Cep, I. Samardzic, *Metalurgija*, 53 (2) (2014) 175-178.
- [21] Q. Wu, S. Zheng, S. Liu, C. Li, Q. Huang, *J. Nucl. Mater.* 442 (2013) 512-517.
- [22] Z. Wu, X. Zhang, X. Song, C. Ma, Y. Qi, X. Chen, Accepted manuscript, *J. Alloys Compd.* (2017).
- [23] G. Golanski, J. Jasak, J. Slania, *Kovove Mater.*, 52 (2) (2014) 99-106.
- [24] M. Mojžiš, L. Domovcová, M. Weiss, M. Fujda, L. Parilák, *Mater. Sci. Forum*, 782 (2014) 133-136.
- [25] L. Falat, A. Výrostková, M. Svoboda, O. Milkovič, *Kovove Mater.*, 49 (6) (2011) 417-426.
- [26] L. Falat, M. Svoboda, A. Výrostková, I. Petryshynets, M. Sopko, *Mater. Character.*, 72 (2012) 15-23.
- [27] M. Lomozik, M. Zeman, R. Jachym, *Kovove Mater.*, 50 (4) (2012) 285-294.
- [28] L. Falat, L. Čiripová, V. Homolová, P. Futáš, P. Ševc, *Kovove Mater.* 54 (6) (2016) 417-427.
- [29] J. Horník, P. Zuna, J. Málek, T. Jetmar, J. Kasl, M. Matějová, F. Jandoš, *Key Eng. Mater.*, 647 (2015) 38-46.
- [30] A. Shibata, T. Murata, H. Takahashi, T. Matsuoka, N. Tsuji, *Metall. Mater. Trans. A*, 46A (12) A (2015) 5685-5696.
- [31] G. Rosenberg, I. Sinaiova, P. Hvizdoš, L. Juhar, *Metall. Mater. Trans. A*, 46A, (10) A (2015) 4755-4771.
- [32] A. Begić Hadžipašić, J. Malina, Š. Nižnik, *Kovove Mater.*, 50 (5) (2012) 345-350.
- [33] M.L. Martin, J.A. Fenske, G.S. Liu, P. Sofronis, I.M. Robertson, *Acta Mater.*, 59 (4) (2011) 1601-1606.
- [34] T. Michler, M.P. Balogh, *Int. J. Hydrogen Energy*, 35 (2010) 9746-9754.

